The effect of ethylcellulose on the rheology and mechanical heterogeneity of asphaltene films at the oil-water interface

Chih-Cheng Chang,[†] Ian Williams,[†,‡] Arash Nowbahar,[†] Vincent Mansard,[†,¶] Jodi Mecca,[§] Kathryn A. Whitaker,[§] Adam K. Schmitt,[§] Christopher J. Tucker ,[§] Tom H. Kalantar,[§] Tzu-Chi Kuo,[§] and Todd M. Squires[*,†]

†*Department of Chemical Engineering, University of California, Santa Barbara, USA*

‡*Department of Chemistry, University College London, 20 Gordon Street, London WC1H 0AJ, UK.*

¶*Laboratory for Analysis and Architecture of Systems, Toulouse, France*

§*The Dow Chemical Company, Midland, USA*

E-mail: squires@engineering.ucsb.edu

Abstract

Asphaltenes are surface-active molecules that exist naturally in crude oil. They adsorb at the water-oil interface and form viscoelastic interfacial films that stabilize emulsion droplets, making water-oil separation extremely challenging. There is thus a need for chemical demulsifiers to disrupt the interfacial asphaltene films, and thereby facilitate water-oil separation. Here, we examine ethycellulose (EC) as a model demulsifier and measure its impact on the interfacial properties of asphaltene films using interfacial shear microrheology. When EC is mixed with an oil and asphaltene solution, it retards the interfacial stiffening that occurs between the oil phase in contact

with a water phase. Moreover, EC introduces relatively weak regions within the film. When EC is introduced to a pre-existing asphaltene film, the stiffness of the films decreases abruptly and significantly. Direct visualization of interfacial dynamics further reveals that EC acts inhomogeneously, and that relatively soft regions in the initial film are seen to expand. This mechanism likely impacts emulsion destabilization, and provides new insight to the process of demulsification.

Introduction

Naturally occurring components of crude oil such as asphaltenes, resins, inorganic particles and waxes can act as surfactants and stabilize emulsions of water in crude oil. Asphaltenes are a class of thousands of distinct molecules defined by their solubility in toluene and insolubility in light alkanes.[1–3] Fraction of asphaltenes are strongly surface active and to therefore form stable interfacial layers.[4–6] Asphaltene adsorption at the water-oil interfaces has been shown to increase the interfacial complex modulus $|G_s^*|$ and to result in a transition from a viscous, liquid-like interface to a more elastic, solid-like interfacial film.[7–10] These viscoelastic interfacial layers can stabilize water-oil emulsions through various mechanisms: via a steric or electrostatic repulsions that prevent two water interfaces from approaching, or by introducing a solid-like boundary that slows film drainage, or by way of a solid-like film that must be ruptured for drops to coalesce.[5,11–13]

The surface rheology of interfacial layers has been hypothesized to correlate with emulsion and foam stability.[13–16] However, emulsion stabilization is a complex phenomenon that involves multiple mechanisms, and the processes connecting of surface rheology to emulsion stability remain correlative rather than directly proven. Zell and coworkers[17,18] found many soluble surfactants to be surface shear inviscid, despite being known as effective stabilizers of emulsions and foams. Harbottle et al. suggest surface elasticity impacts emulsion stability, based on comparing measurements of coalescence time and surface shear elasticity for asphaltene stabilized-drops.[16] Clearly, an elastic film needs to be ruptured for drops to

coalesce. It therefore seems reasonable to expect interfaces with strong surface elasticity to resist coalescence more strongly.

Thermal,[19] mechanical,[20] electrical[21] and chemical[22] methods are widely used to promote water-oil separation. A particularly desirable approach is the use of chemical demulsifiers to separate water and oil by enhancing droplet flocculation and/or coalescence.[2,23] In practice, a combination of chemical and electrical/mechanical methods is typically used.[2,24] Diverse demulsifiers have been reported, including polysiloxane,[25] alkylphenol polyalkoxylated resins,[24] polyurethanes,[24] and PO-EO block copolymers.[26–30] These demulsifiers are usually amphiphilic, and can weaken or displace asphaltene interfacial films formed at the water-oil interface.[13,31–36]

Here, we focus on ethylcellulose (EC), which has been studied as a model demulsifier in simple bottle tests,[37,38] micropipette experiments,[39] microfluidic experiments,[40] contact angle measurements,[41,42] atomic force microscopy (AFM)[36] and molecular dynamics simulation.[43] It has been observed that as EC concentration increases the mutually repulsive asphaletene-coated emulsion drops can be driven to adhere and even coalesce.[37,38] Furthermore, the performance of EC has been shown to depend on its hydrophilic-lipophilic balance (HLB) and molecular structure.[44] AFM measurements have shown that EC can break interfacial asphaltene structures heterogeneously.[36,39]

Because of the hypothesized relationship between interfacial rheology and emulsion stability, it is desirable to characterize the influence of EC on the mechanical properties of an asphaltene interfacial film, and its consequent effect on demulsification. However, to date, little research has focused on this aspect of EC behavior.[35] Our previous study revealed that asphaltene films exhibit micron-scale mechanical heterogeneities, suggesting that asphaltenes form a complicated structure at the water-oil interface.[45] Lin et al. also report that heterogeneity in the interfacial structure influences the rheology of the interfacial layer.[46] Obviously, care must be taken when interpreting rheological changes driven by EC.

Previously, we combined highly sensitive microrheometry with direct visualization to re-

veal micron-scale mechanical heterogeneities in asphaltene layers at the water-oil interface.[45] Building on that work, we now investigate the evolution of interfacial rheology when EC is introduced to an interfacial asphaltene film following two different protocols. In the first protocol, an oil phase containing both asphaltene and EC is mixed and brought into contact with an aqueous phase, forming an oil-water interface. In this way, we investigate the ability of EC to inhibit asphaltene adsorption and prevent the formation of elastic layers at the interface. In the second protocol, a 'drop-in' EC solution is added to a pre-formed and aged asphaltene layer to study the ability of EC to break an existing asphaltene layer. These experiments enable the interfacial shear rheology and local structure near the probe to be characterized simultaneously, revealing an inhomogeneous softening process.

Materials and Methods

Materials

C7 asphaltene is precipitated from bitumen (Alberta, Canada) using n-heptane. Ethylcellulose (EC, STD-100, The Dow Chemical Company) has a number-average molecular weight 57000 g/mol and weight-average molecular weight 179000 g/mol.[47] The oil phase is composed of toluene (Sigma-Aldrich, HPLC grade, purity=99.9%) and decane (Sigma-Aldrich, anhydrous, purity $\geq$99%), mixed at a volume ratio of 1 to 4. This oil phase is a poor solvent for the asphaltenes, which form natural aggregates that gradually sediment to the interface during the rheology measurement. As in our previous study,[45] we exploit these aggregates as tracers to track the interfacial flow fields, and ultimately stiffness heterogeneity. We consider three oil-based solutions: 0.1 wt% C7 asphaltene, 0.01 wt% EC, and a mixture of 0.1 wt% C7 and 0.01 wt% EC. The choices of asphaltene and EC concentration are based on our previous study of asphaltene adsorption[45] and results from the literature on EC performance,[37,39] which indicate that this concentration can disrupt stiff asphaltene films, and destabilize emulsions. These are prepared by dissolving C7 and/or EC in toluene and sonicating for

10 minutes before adding decane and sonicating for an additional 10 minutes. Immediately prior to measurement, the solution is again sonicated for 10 minutes to disperse any asphaltene aggregates. Asphaltene solutions are prepared daily to avoid degradation such as the oxidation.[48,49] The aqueous phase is deionized water (Milli-Q, resistivity 18.2 MΩcm).

Rheological measurement and mapping interfacial heterogeneity

The magnetic microbutton microrheometry technique and the custom water-oil sample cell for interfacial rheology are described in previous publications[17,18,45,50,51] and are summarized here. Figure 1 (a) shows a 10 μm thick, 100 μm diameter disk-like microbutton probe used to measure the shear response of a water-oil interface. The microbutton is amphiphilic due to the SU-8 photoresist and the thiol monolayer, and its ferromagnetism is provided by the nickel layer. The microbutton is deposited at the surface of 400 μl of water in a custom Delrin® sample cell surrounded by the electromagnet array as illustrated in Fig. 1 (b). Figure 1 (c) shows a cross-sectional side view of the electromagnet array and sample cell. The water level in the center channel is pinned by the PTFE tape on the Delrin® cell and tuned via the side channel in order to form a flat surface.

The magnetic moment of the microbutton is calibrated following the method described previously.[45] After calibration, 40μl of the oil phase is deposited on top of the water, forming a water-oil interface. Three oil phases - 0.1 wt% C7, 0.01 wt% EC and a 0.1 w% C7 and 0.01 wt% EC mixture - are used in this study. Asphaltene and/or EC adsorb from the oil phase to the interface resulting in measurable interfacial rheology. In what follows, we compare the interfacial rheology due to a "premixed" C7 and EC solution (Fig. 2 (a)) with that measured when EC is introduced to an aged asphaltene layer (Fig. 2 (b)). The introduction of EC is achieved by first adding 40 μl of oil containing 0.1 wt% C7, allowing the asphaltene film to form and age to the limitation of measurement, then subsequently depositing an additional 40μl of oil containing 0.01 wt% EC. After the oil and water make contact, the microbutton is torqued sinusoidally by a magnetic field generated by an array

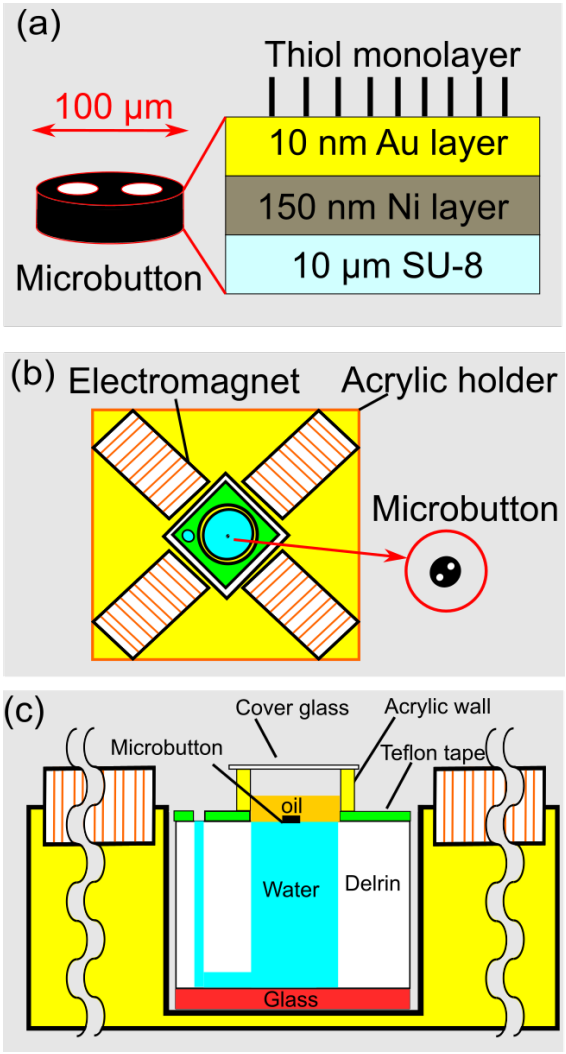

Figure 1: Schematics of the experimental setup (not to scale) (a) Side view of microbutton. The SU-8 photoresist forms the hydrophilic side. Ferromagnetism is a result of the 150 nm nickel layer. A gold layer anchors a hydrophobic thiol monolayer. (b) Top view of the electromagnet array. Four electromagnets are placed in an acrylic holder around a custom Delrin® sample cell. (c) Side view of the sample cell. The water level in the central channel is pinned by the polytetrafluoroethylene (PTFE) tape and controlled via the side channel. The microbutton is placed in the central channel. The acrylic wall and cover glass prevent evaporation.

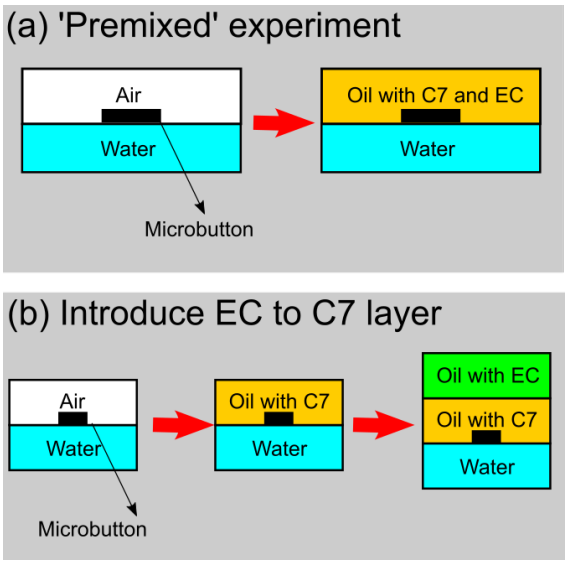

Figure 2: (a) The 'premixed' experiment. An oil phase containing both C7 and EC is placed on top of water, forming an oil-water interface onto which asphaltene and EC adsorb simultaneously. (b) EC is introduced to a pre-existing C7 layer. First, oil containing only C7 is placed on water and an asphaltene film is allowed to form. Subsequently, a second layer of oil containing EC is carefully added, allowing the EC to interact with a preformed C7 layer.

of electromagnets. A custom LabVIEW program controls the magnetic field and records the corresponding probe response. Additionally, the interface and microbutton are visualized via bright-field microscopy (Eclipse 80i, Nikon) using a CCD camera (CV-A10CL, JAI) to track the microbutton rotation.

The applied magnetic torque, $\Gamma \approx mB_0e^{i\omega t}$, and measured angular displacement of the probe, $\Delta\theta(t) = \Delta\theta_0 e^{i(\omega t-\delta)}$, are obtained simultaneously. Here m is the magnetic moment, B_0 is the amplitude of the oscillating magnetic field, ω is angular frequency, t is time, $\Delta\theta_0$ is the amplitude of the probe rotation, and δ is a phase lag relative to the torque. Frequency is fixed at 1 Hz, and $\Delta\theta_0$ is held below 0.3%±0.02% ($\sim 1°$) by controlling B_0 to prevent yielding of the interface. The rotational drag resistance ξ_R^* is defined to be:

$$\xi_R^* = \frac{mB_0e^{i\delta}}{i\omega\Delta\theta_0}, \tag{1}$$

and in general results from both interfacial and bulk contributions. The Boussinesq number,

Bo, characterizes the relative contributions of interfacial and bulk drag. For a rotating cylindrical probe, Bo is given by:

$$Bo = \frac{\eta_s}{\eta a}, \tag{2}$$

where η is the sum of the viscosities of the two bulk phases, η_s is the interfacial viscosity, and a is the radius of the probe.[52] When $Bo \gg 1$, interfacial drag dominates and drag from bulk phases can be neglected. Hughes et al.[52] have shown that the rotational drag resistance of a cylinder at an interface is $\xi_R = 4\pi\eta_s a^2$ when $Bo \gg 1$. Comparing this with equation (1) gives the interfacial complex viscosity in the high Bo regime:

$$\eta_s^* = \frac{mB_0 e^{i\delta}}{i\omega\Delta\theta_0 4\pi a^2}, \tag{3}$$

The interfacial complex modulus, G_s^*, is then

$$G_s^*(\omega) = i\omega\eta_s^*(\omega) = \frac{mB_0}{4\pi a^2\Delta\theta_0}\left(\cos\delta + i\sin\delta\right). \tag{4}$$

In this study, the rheological response is characterized by $|G_s^*|$ and δ, representing the overall stiffness and the viscoelastic nature of the interface respectively. In-phase probe motion, $\delta = 0$, indicates elastic behavior, while $\delta = \pi/2$ reflects a purely viscous response. Intermediate values of δ represent a viscoelastic interface.

The characterization of local stiffness and rheological heterogeneity is described in our previous study.[45] The C7 asphaltene forms aggregates at the interface which serve as natural tracers. In experiments using only EC, no aggregates are observed, and so we instead disperse polyethylene particles (Cospheric, diameter 1 to 4 μm) on the water surface before the oil is deposited. These particles act as artificial tracers. The angular displacement of tracers (aggregates or PE particles), $\Delta\theta$, is tracked[53] as a function of time and distance from the probe center, r. A fast Fourier transform (FFT) is applied to $\Delta\theta(t, r)$ to obtain the angular displacement amplitude as a function of frequency and the amplitude at 1 Hz is extracted

to map the angular strain field.

The decay of angular strain with distance from a rotating cylinder reflects the Boussinesq number.[54] For a homogeneous interface and $Bo \gg 1$, interfacial drag dominates, and the angular strain decays according to

$$\frac{\Delta\theta(r)}{\Delta\theta_0} = \left(\frac{r}{a}\right)^{-2} \tag{5}$$

This interface-dominated behavior represents interfacial films that deforms under shear. When the probe shears these films, and provide a stronger resistance to shear than the bulk water and oil phases on either side. In the limit of $Bo \ll 1$, the interface is relatively soft and bulk drag dominates. For $r \gg a$, the strain decay is approximately

$$\frac{\Delta\theta}{\Delta\theta_0} \sim \frac{4}{3\pi}\left(\frac{r}{a}\right)^{-3}. \tag{6}$$

The bulk-phase dominated regions are ones where the film is weak enough that the viscous resistance from the oil and water phase dominates the overall resistance.

Rigid body rotation occurs when regions are much stiffer than their surroundings so rotating without deforming, and shear surrounding. For example, asphaltenes have been reported to form rigid films at the interface by building a cross-linked network structure[12] If the interface behaves as a rigid body that rotates with the probe, no strain decay is measured:

$$\frac{\Delta\theta}{\Delta\theta_0} = \text{constant}. \tag{7}$$

We have previously shown that a C7 asphaltene film is not homogeneous, but instead exhibits micron-scale variations in local stiffness.[45] To characterize local stiffness, we define an apparent decay exponent, n_{app}, for each aggregate, that corresponds to the effective

power-law decay exponent that would give rise to the observed strain:

$$n_{app} = \frac{\log\left(\frac{\Delta\theta}{\Delta\theta_0}\right)}{\log\left(\frac{r}{a}\right)}. \tag{8}$$

For simplification, n_{app} is sorted into three quantitative categories. Very rapid decay ($n_{app} < -3$) is termed bulk-dominated, intermediate decay ($-1 > n_{app} > -3$) corresponds to interface-dominated, and slow decay ($n_{app} > -1$) represents rigid-body. Local stiffness maps illustrating rheological heterogeneity are created by coloring the Voronoi cells of each aggregate based on its discretized n_{app}. Red, green and blue represent rigid, interface-dominated and bulk phase-dominated regions, respectively.

Results and discussion

Concurrent adsorption of asphaltene and EC

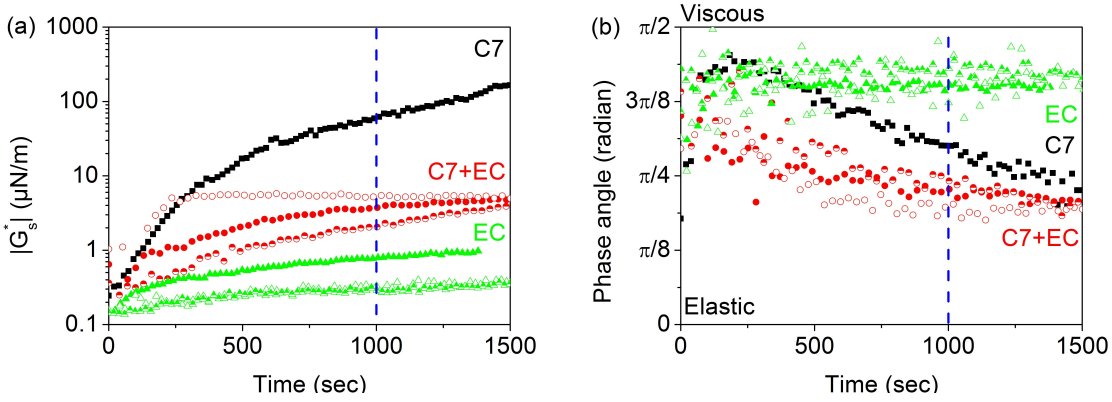

Figure 3: (a) Evolution of the magnitude of the interfacial complex modulus when the oil phase contains 0.1 wt% C7 asphaltene (black), 0.1 wt% C7 and 0.01 wt% EC (red) and 0.01 wt% EC (green). Different symbols with identical color represent multiple trials, prepared and conducted identically. (b) Evolution of the phase angle in the same experiments. The blue dashed line represents the sampling time in Figure 4.

We first investigate the impact of EC on C7 asphaltene adsorption when both are present in solution and concurrently adsorb to the interface. Figure 3 shows $|G_s^*|$ and δ as a function

of time for oil phases containing 0.1 wt% C7 (black), premixed 0.1 wt% C7 and 0.01 wt% EC (red) and 0.01 wt% EC (green). Interfaces between water and oil with asphaltene only stiffen 1000-fold in 1500 seconds, with the phase angle δ decreasing steadily, indicating that the interface transitions from a viscous- to a more elastic-dominated response. We have previously established that stiffening of the interface varies from experiment to experiment due to the mechanical heterogeneity on the probe length scale.[45] However, the qualitative trend of increasing stiffness and elasticity is reproducible and robust.

Qualitatively different behavior is observed for EC solutions in the oil phase (green). Namely, the interfacial stiffness increases only 5-10 times over 1500 seconds as EC adsorbs, and retains a viscous-dominated nature ($\delta(t) \sim \frac{\pi}{2}$). Mixed EC and C7 solution in oil phase, however, show an intermediate behavior. This is accompanied by a transition from viscous- to elastic-dominated behavior, much like pure C7.

The rheological measurements during concurrent adsorption imply that EC does not entirely prevent C7 adsorption. If EC were to quickly adsorb to the interfacial layer, and to exclude all C7 adsorption, the corresponding viscoelastic response would resemble that of a pure EC layer. Measured surface moduli in Fig. 3 (a) are not consistent with this expectation, as films formed from C7/EC solutions are stiffer than those from pure EC solutions. Moreover, phase angles (Figure 3 (b)) for EC films remain primarily viscous, whereas those for C7/EC mixtures are much more viscoelastic. While it is possible that asphaltenes form a second film on top of a pure EC layer, we would expect such asphaltene films to stiffen like pure asphaltene films. From Fig. 3 (a), the surface moduli $|G_s^*|$ of C7/EC films remains around 5 μN/m, whereas pure C7 films stiffen to $\sim$200 μN/m. Although the phase angles δ measured for C7/EC films seem consistently lower than for C7 films (Fig. 3 (b)), the heterogeneous nature of C7 adsorption[45] showed phase angles for C7 films varied from $3\pi/8$ to $\pi/8$ following $\sim$1000 seconds of adsorption. The apparent difference in phase angle between pure C7 and pre-mixed C7/EC films may therefore not be significant. A plausible interpretation of these data is that EC slows asphaltene adsorption, and interferes

with asphaltene structure formation. Nevertheless, both asphaltenes and EC do adsorb and occupy interfacial area, and therefore compete for limited area at the interface. Consequently, after comparable adsorption times, we measure stiffnesses which are intermediate between pure C7 and pure EC, but exhibit a viscoelastic character comparable to pure C7. In what follows, we will show that both the stiff and soft regions coexist at the premixed interface.

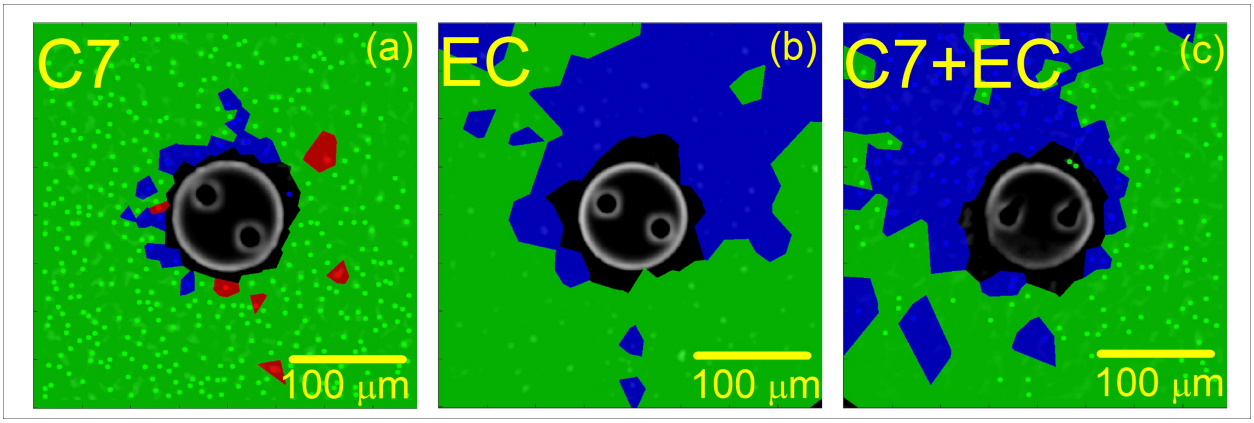

Figure 4: Local viscoelastic character of aged interfaces after 1000 seconds of adsorption of (a) C7, (b) EC, and (c) mixed C7 and EC. Red, green and blue represent rigid-body, interface-dominated, and bulk phase-dominated rotation respectively.

Figure 4 maps the apparent decay exponent, n_{app}, defined in equation (8), corresponding to the rheological measurements in Fig. 3 after 1000 seconds of adsorption. Figure 4 (a) shows the local rheological character for the pure asphaltene layer (black rectangles in Fig. 3 (a)). The viscoelastic character is primarily interface-dominated, indicating that adsorbed asphaltenes form a stiff interfacial layer responsible for the drag resistance measured in Fig. 3 (a). Figure 4 (b) illustrates n_{app} for pure EC adsorption (red closed circles in Fig.3 (a)). EC adsorption forms a heterogeneous film with mixed bulk-phase-dominated and interface-dominated regions. This implies that some regions of a pure EC interface have less surface-active material, or weaker interfacial structure, than others and remain relatively soft, resulting in the relatively lower $|G_s^*|$ measured in Fig. 3 (a).

Figure 4 (c) shows n_{app} following the concurrent adsorption of C7 and EC (green closed triangles in Fig 3 (a)). This mixed system also exhibits coexistence of bulk-phase-dominated and interface-dominated regions, suggesting that EC can prevent C7 from forming a stiff

interfacial layer. The observed heterogeneity can explain the variations in $|G_s^*|$ between nominally identical experiments, since the measured $|G_s^*|$ depends on the rheological environment local to the probe. Furthermore, this rheological heterogeneity can explain the lower overall $|G_s^*|$, compared with pure C7 adsorption, since bulk-dominated regions offer less resistance to interfacial shear.

These data suggest that EC can create soft regions whether or not C7 is present. That $|G_s^*|$ is higher when both C7 and EC adsorb than when EC adsorbs, indicates that the interface-dominated regions in the premixed experiments are stiffer than those resulting from pure EC adsorption. It is clear that when C7 and EC adsorb simultaneously, EC retards C7 adsorption and forms a softer interfacial layer than pure C7 adsorption. Furthermore, whenever EC is adsorbed, the interface is mechanically heterogeneous, consisting of softer bulk-phase-dominated and stiffer interface-dominated regions on the length scale of our probe. This heterogeneous interfacial layer can vary from trial to trial, even with interfaces prepared identically. This phenomena is also manifested in the quantitative differences in the rheological responses of these films.

In order to assess the generality of this observation, we consider the time evolution of the area fractions of rigid, interface-dominated and bulk-phase dominated regions in multiple indentically-prepared experiments. Figure 5 shows the average time evolution for each of the distinct adsorption experiments (pure C7, pure EC, and premixed C7 and EC). The area fraction evolution for each individual experiment are shown in the Supplementary Information Figs. S1-S3.

For pure C7 adsorption, Fig. 5 (a) shows a fast initial increase in interface-dominant rheology from around 70% to 90% of the interfacial area. The bulk-phase-dominated area correspondingly decreases from around 25% to 5% and a small increase in rigid area is suggested. By comparison, pure EC adsorption (Fig. 5 (b)) reveals no rigid regions, and only bulk-phase-dominated and interface-dominated area respectively. Notably, however, the interface-dominated area fraction is observed to increase slowly and steadily from ap-

proximately 60% to 80%. Finally, Fig. 5 (c) illustrates this evolution for premixed C7 and EC. Bulk-phase-dominated and interface-dominated regions coexist, and a slow increase in the proportion of interface-dominated region from around 30% to 70% is measured. That the increase in the interface-dominated area occurs significantly more slowly when C7 and EC adsorb concurrently compared to the pure C7 case suggests that the presence of EC does indeed retard asphaltene adsorption. The end-state in the mixed system consists of a significantly larger proportion of bulk-phase-dominated area and reduced rigid area compared to the pure C7 experiments. This result supports our speculation that, in addition to its retarding effect, EC modifies and weakens the structure of the asphaltene film. Thus, the effect of EC on the C7 film appears to be two-fold: EC both slows asphaltene adsorption and alters its interfacial structure.

EC introduction to aged Asphaltene Layers

Having demonstrated the effect of simultaneously EC on C7 adsorption when they adsorb simultaneously from a premixed solution, we now investigate the effect of adding EC to an aged C7 asphaltene layer using the procedure described in Fig. 2. Figure 6 shows the evolution of $|G_s^*|$ and δ before and after a 0.01 wt% EC solution is introduced to an asphaltene layer formed by adsorption from a 0.1 wt% C7 solution. We initially monitor C7 adsorption until $|G_s^*|$ reaches the upper limit of measurement, set by the magnetic moment of the probe (which varies trial to trial), and then introduce the EC solution (at time $t = 0$). The large symbols at $t < 0$ reflect the rheology as pure C7 adsorbs, whereas the small symbols at $t > 0$ show the rheological evolution after adding EC.

Figure 6 (a) shows that interfacial shear moduli are weakened by 1-3 orders of magnitude after introducing EC to the aged C7 layer. Following this initial decrease, however, qualitative variation arise between nominally identical experiment. Some interfaces (blue, orange and green) continue to soften, while one (purple) gradually recovers to high $|G_s^*|$, and one (red) appears arrested at an intermediate stiffness.

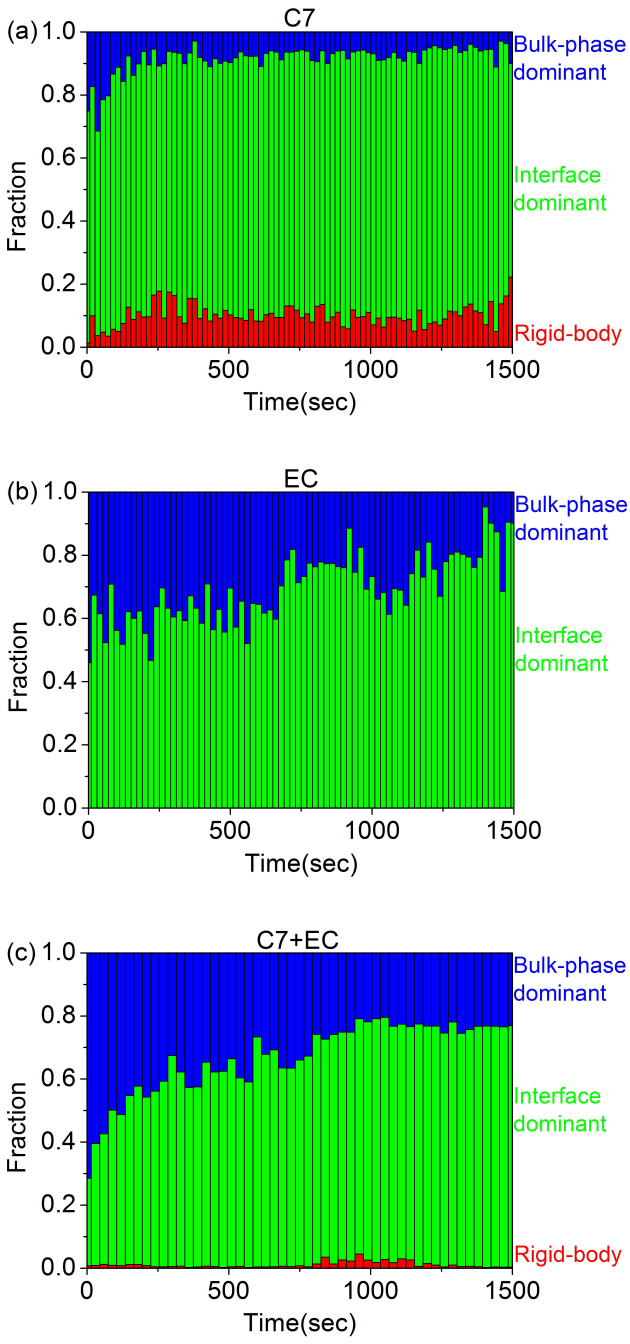

Figure 5: Evolution of average area fraction of rigid-body (red), interface-dominated (green) and bulk-phase dominated (blue) regions for (a) C7 only, (b) EC only and (c) premixed C7 and EC interface.

Figure 6 (b) demonstrates that, in all experiments, the phase angle δ increases immediately after depositing EC, corresponding to loss of elasticity. Following this immediate increase, δ remains high in those experiments for which $|G_s^*|$ continues to decrease (blue, orange and green), indicating that more liquid-like behavior is maintained. This phenomena contrasts with those experiments for which $|G_s^*|$ recovers or appears arrested (red and purple, respectively), in which δ slowly decreases as the rheological character of the interface transitions back towards an elastic response. Thus, the long-time scale recovery of interfacial stiffness is associated with a recovery of elastic behavior. EC successfully softens the aged C7 asphaltene layers, but with qualitative and quantitative variations after the initial softening. This variation likely reflects the heterogeneity of the asphaltene film on the length scale of our microbutton probe, with certain areas of the asphaltene layer more susceptible to penetration and disruption by EC than others.

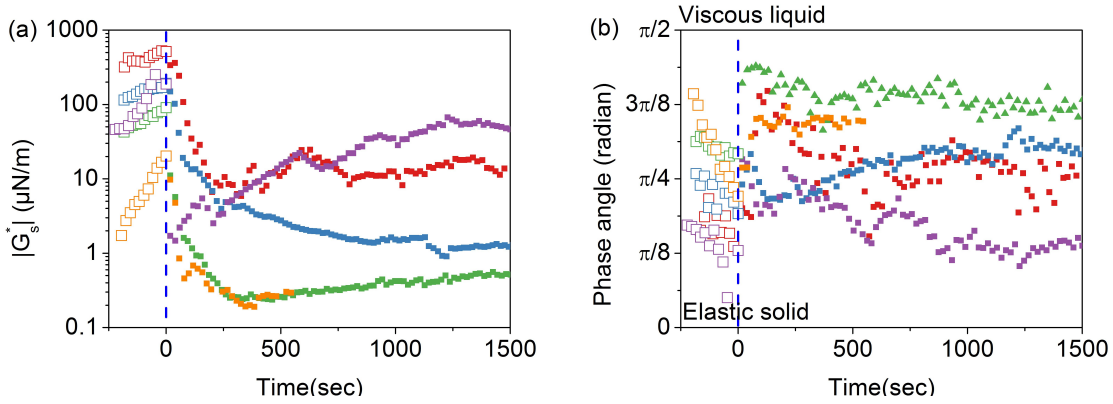

Figure 6: (a) Evolution of the magnitude of the interfacial complex modulus when a 0.01 wt% EC solution is deposited above an aged asphaltene interface formed from a 0.1 wt% C7 solution. Different colors represent multiple trials prepared and conducted identically. EC is introduced at $t = 0$. (b) Evolution of the phase angle in the same experiments. Large (small) symbols show quantities before (after) EC addition. Different colors represent different trials using identical experimental procedure.

In order to investigate the effect and evolution of mechanical heterogeneity, Fig. 7 shows maps of local stiffness in a single experiment (orange data in Fig. 6) before and after depositing EC. Figure 7 (a) re-plots $|G_s^*|(t)$ for this experiment, emphasizing the early stages

of evolution, and indicating the five points considered in panels (b-f). Figure 7 (b) shows the map of n_{app} immediately prior to EC addition and Figure 7 (c)-(f) show the evolution of this map. As evident from Fig. 7 (b), the interface is initially mechanically heterogeneous with a scar-like soft region near the probe and a rigid-body-like region in the lower left of the field of view. After EC is introduced, the pre-existing soft, bulk-phase-dominated region expands (Fig. 7 (c), (d) and (f)). As this occurs, $|G_s^*|$ decreases as drag resistance in the vicinity of the probe is decreased. After a long time, Fig. 7 (f) indicates that interface-dominated regions gradually recover, but the region near the probe remains soft.

The evolution of n_{app} in Fig. 7 suggests that EC preferentially impacts regions which are already soft. EC may more easily penetrate, disrupt or expand weak regions in the pre-existing asphaltene film. That EC has the ability to displace and disrupt asphaltene interfacial layer agrees with the literature studies.[55,56] The recovery of the interface-dominated region implies that bulk C7 might adsorb back into the soft region created by EC, or that a restructuring of the interfacial layer occurs, increasing the film stiffness.

Averaging the instantaneous area fractions of bulk-phase-dominated, interface-dominated and rigid-body-like regions obtained from five identically prepared experiments in which EC is added to a pre-existing asphaltene layer at $t = 0$ reveals the general evolution of mechanical heterogeneity shown in Figure 8. The evolution of each trial is shown in the Supplementary Information Fig. S4. The interface-dominated and rigid-body fraction decrease rapidly when EC is introduced, while the bulk-phase-dominated regions increase. After this initial expansion of bulk-phase-dominated regions and associated softening, the interface slowly begins to recover towards a more interface-dominated drag resistance. This trend supports the generality of the progression shown in the maps in Fig. 7, and explains the data in Fig. 6.

Although the general trend appears robust, qualitative differences in evolution are observed between independent trials. The experiments in which interfacial stiffness increases or remains at intermediate value after its initial drop (red and purple data in Fig. 6) exhibit a

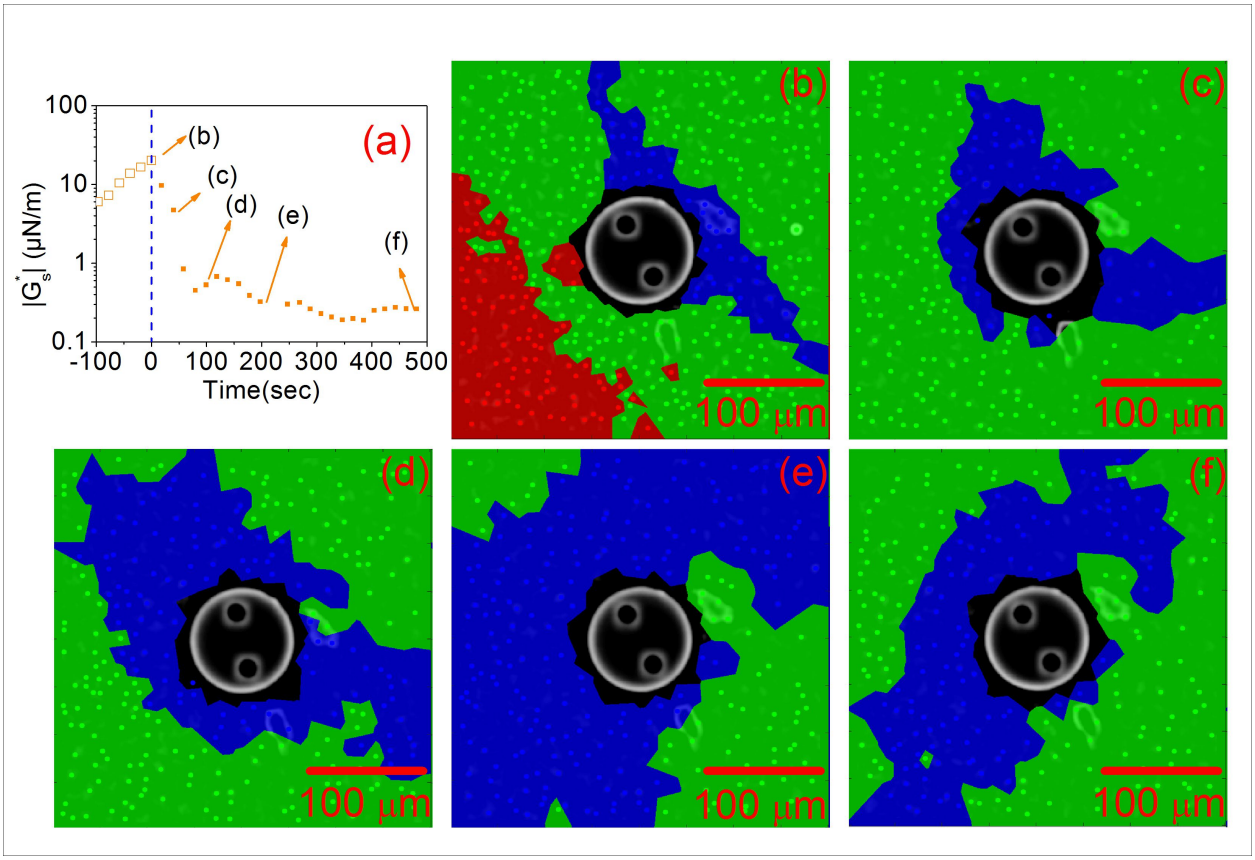

Figure 7: (a) Interfacial rheology of the water-oil interface when adding 0.01 wt% EC to an aged asphaltene layer. EC is introduced at $t = 0$. (b) Mechanical local stiffness before adding EC. (c)-(f) Evolution of mechanical local stiffness after adding EC. Red, green and blue cells represent rigid-body rotation, interface-dominated rotation and bulk phase-dominated rotation, respectively.

much faster recovery of the interface-dominated area fraction compared to those experiments in which interfacial stiffness continues to decrease over a much longer period (blue and green data in Fig. (6). It is likely that differences in the local structure near the probe determine the differences in the measured rheology.

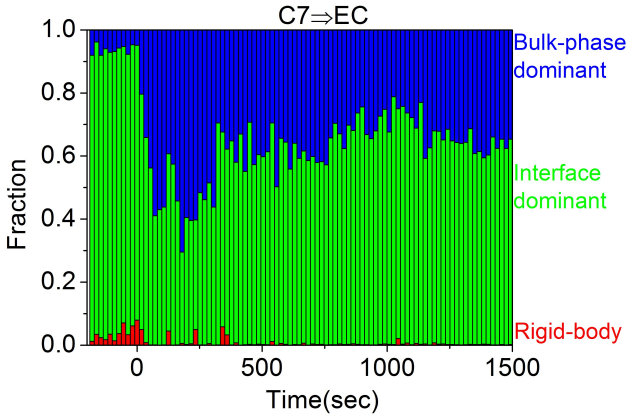

Figure 8: Evolution of average area fractions of rigid-body (red), interface-dominated (green) and bulk-phase-dominated (blue) regions after introducing 0.01 wt% EC on aged C7 layer. EC is deposited at $t = 0$. Data are an average of five identically prepared experiments.

Conclusion

We have studied the effect of ethylcellulose (EC) on the rheology of a C7 asphaltene film at an oil-water interface in two distinct situations. When asphaltenes and EC are both present in solution and adsorb simultaneously, EC slows the adsorption of asphaltenes, and disrupts the formation of interfacial structures, resulting in softer interfacial layers than these formed from asphaltenes alone. When EC is introduced to a pre-existing asphaltene film, it softens the film in an inhomogeneous manner. Pre-existing soft regions in the initial asphaltene layer are more susceptible to penetration by EC, and expand at the expense of stiff regions, decreasing the measured interfacial stiffness. After this initial softening, the interfacial structure and stiffness may recover.

Although the existence of structural and rheological heterogeneity in asphaltene films is well established, this work represents the first experimental demonstration of the conse-

quences of this heterogeneity for chemical demulsification. We have shown that chemical demulsifiers are likely to target or to impact most strongly the relatively soft regions within asphaltene films. The fact that interfacial stiffness recovers following a fast initial softening, suggests that there may be a limited timescale on which an emulsion can be broken after the addition of a demulsifier.

Acknowledgement

We acknowledge primary support for this project from The Dow Chemical Company through their University Partnership Initiative (UPI), and an NSF Graduate Research Fellowship Program under Grant DGE-1144085 (for AN). Any opinion, findings, and conclusions or recommendations expressed in this material are those of the authors and do not necessarily reflect the views of the National Science Foundation. Portions of this work were performed using the shared experimental facilities of the Materials Research Science and Engineering Center at UCSB (MRSEC NSF DMR 1720256), the UCSB Nanofabrication Facility, part of the NSF NNIN network, and the Microfluidics Lab within The California NanoSystems Institute (CNSI) supported by UCSB and the UC Office of the President.

Supporting Information Available

This manuscript contains supporting information:

Figure S1: Three identical experimental trials of evolution of area fraction for calculating the average value of Fig. 5 (a).

Figure S2: Three identical experimental trials of evolution of area fraction for calculating the average value of Fig. 5 (b).

Figure S3: Three identical experimental trials of evolution of area fraction for calculating the average value of Fig. 5 (c).

Figure S4: Five identical experimental trials of evolution of area fraction for calculating the average value of Fig. 8.

References

(1) Mullins, O. C. The asphaltenes. *Annual review of analytical chemistry (Palo Alto, Calif.)* **2011**, *4*, 393–418.

(2) Kokal, S. Crude Oil Emulsions: A State-Of-The-Art Review. *SPE Production & Facilities* **2005**, *20*, 5–13.

(3) Schuler, B.; Meyer, G.; Peña, D.; Mullins, O. C.; Gross, L. Unraveling the Molecular Structures of Asphaltenes by Atomic Force Microscopy. *Journal of the American Chemical Society* **2015**, *137*, 9870–9876.

(4) Rane, J. P.; Pauchard, V.; Couzis, A.; Banerjee, S. Interfacial Rheology of Asphaltenes at Oil-Water Interfaces and Interpretation of the Equation of State. *Langmuir* **2013**, *29*, 4750–4759.

(5) Spiecker, P. M.; Kilpatrick, P. K. Interfacial rheology of petroleum asphaltenes at the oil-water interface. *LANGMUIR* **2004**, *20*, 4022–4032.

(6) Sjoblom, J.; Aske, N.; Harald, I.; Brandal, Ø.; Erik, T.; Sæther, Ø. Our current understanding of water-in-crude oil. Recent characterization techniques and high pressure performance. *Advances in colloid and interface science* **2003**, *102*, 399–473.

(7) Fan, Y.; Simon, S.; Sjöblom, J. Interfacial shear rheology of asphaltenes at oil-water interface and its relation to emulsion stability: Influence of concentration, solvent aromaticity and nonionic surfactant. *Colloids and Surfaces A: Physicochemical and Engineering Aspects* **2010**, *366*, 120–128.

(8) Verruto, V. J.; Le, R. K.; Kilpatrick, P. K. Adsorption and molecular rearrangement of amphoteric species at oil-water interfaces. *Journal of Physical Chemistry B* **2009**, *113*, 13788–13799.

(9) Bi, J.; Yang, F.; Harbottle, D.; Pensini, E.; Tchoukov, P.; Simon, S.; Sjöblom, J.; Dabros, T.; Czarnecki, J.; Liu, Q.; Xu, Z. Interfacial Layer Properties of a Polyaromatic Compound and its Role in Stabilizing Water-in-Oil Emulsions. *Langmuir* **2015**, *31*, 10382–10391.

(10) Pradilla, D.; Simon, S.; Sjöblom, J.; Samaniuk, J.; Skrzypiec, M.; Vermant, J. Sorption and Interfacial Rheology Study of Model Asphaltene Compounds. *Langmuir* **2016**, *32*, 2900–2911.

(11) Eley, D. D.; Hey, M. J.; Lee, M. A. Rheological studies of asphaltene films adsorbed at the oil/water interface. *Colloids and Surfaces* **1987**, *24*, 173–182.

(12) Yarranton, H. W.; Sztukowski, D. M.; Urrutia, P. Effect of interfacial rheology on model emulsion coalescence. I. Interfacial rheology. *Journal of Colloid and Interface Science* **2007**, *310*, 246–252.

(13) Pensini, E.; Harbottle, D.; Yang, F.; Tchoukov, P.; Li, Z.; Kailey, I.; Behles, J.; Masliyah, J.; Xu, Z. Demulsification Mechanism of Asphaltene-Stabilized Water-in-Oil Emulsions by a Polymeric Ethylene Oxide-Propylene Oxide Demulsifier. *Energy & Fuels* **2014**, *28*, 6760–6771.

(14) Harvey, P. A.; Nguyen, A. V.; Jameson, G. J.; Evans, G. M. Influence of sodium dodecyl sulphate and Dowfroth frothers on froth stability. *Minerals Engineering* **2005**, *18*, 311–315.

(15) Yarranton, H. W.; Urrutia, P.; Sztukowski, D. M. Effect of interfacial rheology on model emulsion coalescence: II. Emulsion coalescence. *Journal of Colloid and Interface Science* **2007**, *310*, 253–259.

(16) Harbottle, D.; Chen, Q.; Moorthy, K.; Wang, L.; Xu, S.; Liu, Q.; Sjoblom, J.; Xu, Z. Problematic stabilizing films in petroleum emulsions: Shear rheological response of viscoelastic asphaltene films and the effect on drop coalescence. *Langmuir* **2014**, *30*, 6730–6738.

(17) Zell, Z. A.; Nowbahar, A.; Mansard, V.; Leal, L. G.; Deshmukh, S. S.; Mecca, J. M.; Tucker, C. J.; Squires, T. M. Surface shear inviscidity of soluble surfactants. *Proceedings of the National Academy of Sciences of the United States of America* **2014**, *111*, 3677–3682.

(18) Zell, Z. A.; Mansard, V.; Wright, J.; Kim, K.; Choi, S. Q.; Squires, T. M. Linear and nonlinear microrheometry of small samples and interfaces using microfabricated probes. *Journal of Rheology* **2016**, *60*, 141–159.

(19) Fang, C. S.; Chang, B. K.; Lai, P. M.; Klaila, W. J. Microwave demulsification. *Chemical Engineering Communications* **1988**, *73*, 227–239.

(20) Frising, T.; Noïk, C.; Dalmazzone, C. The liquid/liquid sedimentation process: From droplet coalescence to technologically enhanced water/oil emulsion gravity separators: A review. *Journal of Dispersion Science and Technology* **2006**, *27*, 1035–1057.

(21) Eow, J. S.; Ghadiri, M.; Sharif, A. O.; Williams, T. J. Electrostatic enhancement of coalescence of water droplets in oil: A review of the current understanding. *Chemical Engineering Journal* **2001**, *84*, 173–192.

(22) Rondón, M.; Bouriat, P.; Lachaise, J.; Salager, J. L. Breaking of water-in-crude oil emulsions. 1. Physicochemical phenomenology of demulsifier action. *Energy and Fuels* **2006**, *20*, 1600–1604.

(23) Sjöblom, J. *Enzyklopädisches Handbuch zur Emulsionstechnologie*; 2001; p I.

(24) Peña, A. A.; Hirasaki, G. J.; Miller, C. A. Chemically induced destabilization of water-in-crude oil emulsions. *Industrial and Engineering Chemistry Research* **2005**, *44*, 1139–1149.

(25) Dalmazzone, C.; Noik, C.; Komunjer, L. Mechanism of Crude-Oil/Water Interface Destabilization by Silicone Demulsifiers. *SPE Journal* **2005**, *10*, 44–53.

(26) Zhang, Z.; Xu, G.; Wang, F.; Dong, S.; Chen, Y. Demulsification by amphiphilic dendrimer copolymers. *Journal of Colloid and Interface Science* **2005**, *282*, 1–4.

(27) Riess, G.; Labbe, C. Block Copolymers in Emulsion and Dispersion Polymerization. *Macromolecular Rapid Communications* **2004**, *25*, 401–435.

(28) Barnes, T. J.; Prestidge, C. A. PEO-PPO-PEO block copolymers at the emulsion droplet-water interface. *Langmuir* **2000**, *16*, 4116–4121.

(29) Wu, J.; Xu, Y.; Dabros, T.; Hamza, H. Effect of EO and PO positions in nonionic surfactants on surfactant properties and demulsification performance. *Colloids and Surfaces A: Physicochemical and Engineering Aspects* **2005**, *252*, 79–85.

(30) Le Follotec, A.; Pezron, I.; Noik, C.; Dalmazzone, C.; Metlas-Komunjer, L. Triblock copolymers as destabilizers of water-in-crude oil emulsions. *Colloids and Surfaces A: Physicochemical and Engineering Aspects* **2010**, *365*, 162–170.

(31) Mukherjee, S.; Kushnick, A. P. *Oil-Field Chemistry*; Chapter 19, pp 364–374.

(32) Krawczyk, M. A.; Wasan, D. T.; Shetty, C. S. Chemical Demulsification of Petroleum Emulsions Using Oil-Soluble Demulsifiers. *Industrial and Engineering Chemistry Research* **1991**, *30*, 367–375.

(33) Bhardwaj, A.; Hartland, S. Study of demulsification of water-in-crude oil emulsion. *Journal of Dispersion Science and Technology* **1993**, *14*, 541–557.

(34) Ese, M. H.; Sjöblom, J.; Djuve, J.; Pugh, R. An atomic force microscopy study of asphaltenes on mica surfaces. Influence of added resins and demulsifiers. *Colloid and Polymer Science* **2000**, *278*, 532–538.

(35) Yang, F.; Tchoukov, P.; Qiao, P.; Ma, X.; Pensini, E.; Dabros, T.; Czarnecki, J.; Xu, Z. Studying demulsification mechanisms of water-in-crude oil emulsions using a modified thin liquid film technique. *Colloids and Surfaces A: Physicochemical and Engineering Aspects* **2018**, *540*, 215–223.

(36) Hou, J.; Feng, X.; Masliyah, J.; Xu, Z. Understanding interfacial behavior of ethylcellulose at the water-diluted bitumen interface. *Energy and Fuels* **2012**, *26*, 1740–1745.

(37) Feng, X.; Xu, Z.; Masliyah, J. Biodegradable polymer for demulsification of water-in-bitumen emulsions. *Energy and Fuels* **2009**, *23*, 451–456.

(38) Roostaie, T.; Farsi, M.; Rahimpour, M. R.; Biniaz, P. Performance of biodegradable cellulose based agents for demulsification of crude oil: Dehydration capacity and rate. *Separation and Purification Technology* **2017**, *179*, 291–296.

(39) Feng, X.; Mussone, P.; Gao, S.; Wang, S.; Wu, S. Y.; Masliyah, J. H.; Xu, Z. Mechanistic study on demulsification of water-in-diluted bitumen emulsions by ethylcellulose. *Langmuir* **2010**, *26*, 3050–3057.

(40) Nowbahar, A.; Whitaker, K.; Schmitt, A. K.; Kuo, T.-C. Mechanistic Study of Water Droplet Coalescence and Flocculation in Diluted Bitumen Emulsions with Additives Using Microfluidics. *Energy & Fuels* **2017**, *31*, 10555–10565.

(41) Wang, S. Q.; Segin, N.; Wang, K.; Masliyah, J. H.; Xu, Z. H. Wettability Control Mechanism of Highly Contaminated Hydrophilic Silica/Alumina Surfaces by Ethyl Cellulose. *Journal of Physical Chemistry C* **2011**, *115*, 10576–10587.

(42) He, L.; Lin, F.; Li, X.; Xu, Z.; Sui, H. Enhancing heavy oil liberation from solid surfaces using biodegradable demulsifiers. *Journal of Environmental Chemical Engineering* **2016**, *4*, 1753–1758.

(43) Liu, J.; Zhao, Y.; Ren, S. Molecular Dynamics Simulation on Self-Aggregation of Asphaltenes at Oil- Water Interface : Formation and Destruction of the Asphaltene Protective Film. *Energy & Fuels* **2015**,

(44) Feng, X.; Wang, S.; Hou, J.; Wang, L.; Cepuch, C.; Masliyah, J.; Xu, Z. Effect of hydroxyl content and molecular weight of biodegradable ethylcellulose on demulsification of water-in-diluted bitumen emulsions. *Industrial and Engineering Chemistry Research* **2011**, *50*, 6347–6354.

(45) Chang, C.-C.; Nowbahar, A.; Mansard, V.; Williams, I.; Mecca, J.; Schmitt, A. K.; Kalantar, T. H.; Kuo, T.-C.; Squires, T. M. Interfacial Rheology and Heterogeneity of Aging Asphaltene Layers at the Water Oil Interface. *Langmuir* **2018**, *34*, 5409–5415.

(46) Lin, Y.-J.; Barman, S.; He, P.; Zhang, Z.; Christopher, G. F.; Biswal, S. L. Combined interfacial shear rheology and microstructure visualization of asphaltenes at air-water and oil-water interfaces. *Journal of Rheology* **2018**, *62*, 1–10.

(47) Inukai, K.; Takahashi, Y.; Murakami, S.; Ri, K.; Shin, W. Molecular weight dependence of ethyl cellulose adsorption behavior on (La, Sr)(Ti, Fe)O3-δ particles in organic solvent pastes and their printing properties. *Ceramics International* **2014**, *40*, 12319–12325.

(48) Maia Filho, D. C.; Ramalho, J. B.; Spinelli, L. S.; Lucas, E. F. Aging of water-in-crude oil emulsions: Effect on water content, droplet size distribution, dynamic viscosity and stability. *Colloids and Surfaces A: Physicochemical and Engineering Aspects* **2012**, *396*, 208–212.

(49) Siddiqui, M. N.; Ali, M. F. Studies on the aging behavior of the Arabain asphalts. *Fuel* **1999**, *78*, 1005–1015.

(50) Choi, S. Q.; Steltenkamp, S.; Zasadzinski, J. A.; Squires, T. M. Active microrheology and simultaneous visualization of sheared phospholipid monolayers. *Nature communications* **2011**, *2*, 312.

(51) Kim, K.; Choi, S. Q.; Zasadzinski, J. A.; Squires, T. M. Interfacial microrheology of DPPC monolayers at the airwater interface. *Soft Matter* **2011**, *7*, 7782–7789.

(52) Hughes, B. D.; Pailthorpe, B. A.; White, L. R. The translational and rotational drag on a cylinder moving in a membrane. *Journal of Fluid Mechanics* **1981**, *110*, 349–372.

(53) Crocker, J.; Grier, D. Methods of Digital Video Microscopy for Colloidal Studies. *Journal of Colloid and Interface Science* **1996**, *179*, 298–310.

(54) Goodrich, F. C. The Theory of Absolute Surface Shear Viscosity. I. *Proceedings of the Royal Society of London. Series A, Mathematical and Physical Sciences* **1969**, *310*, 359–372.

(55) Natarajan, A.; Kuznicki, N.; Harbottle, D.; Masliyah, J.; Zeng, H.; Xu, Z. Molecular Interactions between a Biodegradable Demulsifier and Asphaltenes in an Organic Solvent. *Energy & Fuels* **2016**, *30*, 10179–10186.

(56) Kuznicki, N. P.; Harbottle, D.; Masliyah, J. H.; Xu, Z. Probing Mechanical Properties of Water-Crude Oil Interfaces and Colloidal Interactions of Petroleum Emulsions Using Atomic Force Microscopy. *Energy and Fuels* **2017**, *31*, 3445–3453.

For Table of Contents Use Only